Magnetic Resonance Imaging of drying bitumen emulsions

Marie Goavec, Stéphane Rodts, Vincent Gaudefroy, Pamela Françoise Faure, Philippe Coussot

▶ **To cite this version:**

Marie Goavec, Stéphane Rodts, Vincent Gaudefroy, Pamela Françoise Faure, Philippe Coussot. Magnetic Resonance Imaging of drying bitumen emulsions. Colloids and Surfaces A: Physicochemical and Engineering Aspects, 2020, 591, 22 p. 10.1016/j.colsurfa.2020.124512 . hal-03594425

HAL Id: hal-03594425
https://hal.science/hal-03594425

Submitted on 2 Mar 2022

HAL is a multi-disciplinary open access archive for the deposit and dissemination of scientific research documents, whether they are published or not. The documents may come from teaching and research institutions in France or abroad, or from public or private research centers.

L'archive ouverte pluridisciplinaire **HAL**, est destinée au dépôt et à la diffusion de documents scientifiques de niveau recherche, publiés ou non, émanant des établissements d'enseignement et de recherche français ou étrangers, des laboratoires publics ou privés.

Version of Record: https://www.sciencedirect.com/science/article/pii/S0927775720301059
Manuscript_4e6274533e4b7232639465bb065b919e

Magnetic Resonance Imaging of drying bitumen emulsions

M. Goavec, S. Rodts, V. Gaudefroy*, P. Faure, P. Coussot

Université Paris-Est, Laboratoire Navier (ENPC-IFSTTAR-CNRS), 2 Allée Kepler, 77420 Champs sur Marne, France

* IFSTTAR, MAST, Route de Bouaye, 44344 Bouguenais, France

Abstract: From Magnetic Resonance Imaging (MRI) measurements allowing to distinguish separately the density distribution of the two phases of the system, we show that bitumen emulsions essentially dry homogeneously, with nevertheless a slight concentration gradient increasing towards the sample free surface exposed to air. Remarkably, despite the resulting large concentration of bitumen droplets formed around the free surface of the sample, the bitumen droplets do not coalesce before the very last stages of drying. In parallel the drying rate strongly and continuously decreases, which is attributed to the reduction of the hydraulic network connected to the sample free surface.

1. Introduction

Direct bitumen-in-water emulsions find various applications in industry, as roofing materials, waterproofing coatings, and especially paving materials [1]. Whether for the base course or the surface treatment of a pavement, they can be used for road construction or recycling [2-6]. However, using a bitumen emulsion means incorporating a significant amount of water that must then be extracted, generally by evaporation and drainage, a complex process [7].

In the road pavement domain, the breaking process of bitumen emulsion is a critical stage that rules the bituminous material behavior. This process is due to bitumen interactions with the mineral aggregates or to water loss, or both. In the case of non-reactive aggregates with emulsion (i.e. acid rock with a high content of silica), the drying of the significant amount of water linked to bitumen emulsion (up to 8% of the mixture weight) strongly influences the rise in cohesion and the curing process of cold mixes. A better understanding of how water is removed from the granular mixture treated with bitumen emulsion is required. Quick drying bitumen emulsions have been designed to accelerate the curing process of cold mixes [8] but this can be hindered by the formation of a bitumen layer [9].

The emerging questions are how can a continuous film be finally reached from an initial dispersion of bitumen droplets [10]? Is it by the formation of a continuous film along the free surface, which would then progressively thicken? How does the drying rate evolve and what are the physical mechanisms at the origin of its evolution?

During the drying of a direct emulsion, the continuous phase, i.e. the aqueous solution, evaporates. As a consequence, globally speaking, i.e. without considering possible concentration gradients, the dispersed phase concentrates. This implies that the bitumen droplets approach each other at a closer (average) distance, and for a sufficiently large droplet concentration we expect them to form a (soft) solid structure [9-10]. Under these conditions, we can consider that we are dealing with a solid porous

© 2020. This manuscript version is made available under the Elsevier user license
https://www.elsevier.com/open-access/userlicense/1.0/

medium (i.e. the droplet network [11]) containing a liquid which has to be extracted during the drying process.

In this context it is useful to review first the basic mechanisms [12-19] of drying of non-deformable, homogeneous solid porous structures initially filled with a liquid perfectly wetting the solid. We consider here only convective drying, i.e. samples submitted to a constant air flux along one of their external surface. Typically, when capillary effects are dominant, i.e. for a 3D liquid network with sufficient connections and a pore size sufficient small so as gravity effects are negligible, and with a pure liquid (no elements in suspension), we observe first a long period of constant drying rate (CRP, i.e. Constant Rate Period). This results from two effects: (i) thanks to capillary effects, any extraction of some liquid volume leads to a (homogeneous) redistribution of the liquid throughout the sample, in order to preserve a uniform Laplace pressure at any point in the liquid network (ii) due to this equilibration process, a large density of small liquid patches remains around the sample free surface, which maintains constant the boundary conditions in terms of relative humidity: the evaporation rate, which results from vapor diffusion from this region, thus remains constant. In a second period, when the liquid film size becomes too thin, capillary effects may become unable to re-equilibrate sufficiently rapidly the liquid network with regards to the external evaporation rate. This implies that the liquid close to the free surface of the sample is not replaced so that a dry region tends to develop. In that case, the rate of drying now decreases because before reaching the top surface of the sample and the external air flux, the water vapor molecules have to diffuse first from the first liquid-air interfaces in the sample then through the dry region. During this Falling Rate Period (FRP) the drying rate progressively becomes less dependent on the external air flux. A long CRP associated with a homogeneous desaturation of the sample are effectively observed in model systems for a wide range of pore sizes (from 0.1 mm down to several tens of nanometers [20]), but a homogeneous desaturation was still observed down to nanometric pore size [20].

With emulsions the situation is more complex as we are now dealing with a “soft solid”, which may deform under capillary stresses. This has two consequences: this can more easily induce some significant gradient of concentration, and ultimately induce droplet coalescence, which may lead to the gradual formation of a continuous oil phase [9-10]. There is less information available concerning emulsion drying than for solid porous materials. From MRI (Magnetic Resonance Imaging) it was shown that the concentration distribution remains uniform during drying in a film of the order of 200 μm thick of model emulsion, for low air flux velocity, but a growing gradient develops as the air flux increases [21]. With a much thicker layer of silicone emulsion, a gradient of concentration develops during the drying process, which likely results in a continuous decrease of the drying rate [22]. A critical observation was that, around the upper interface (in contact with air), the surfactants tend to segregate and an oil layer of growing thickness develops as a result of the coalescence of droplets [22-24]. Other works provided insight on some effects associated with the drying of emulsion samples under different conditions. In a 2D emulsion in a capillary, the droplets appear to coalesce either from the front or in the bulk depending on the surfactant concentration [25-26]. For an emulsion layer enclosed between two solid plates a CRP was first observed, followed by a FRP due to the further approach and deformation of the droplets reducing the liquid path [27]. Other works concern the drying of an emulsion drop lying on a solid surface. This may lead to more complex effects since evaporation now occurs from a very large interface of the sample as compared to its volume, so that the effect of heterogeneities can be stronger, leading to coalescence, cracking, crack healing, etc [28-31].

From direct observations and MRI measurements it was recently shown that during the drying of a direct (oil in water) emulsion the whole system essentially concentrates homogeneously, which leads to shrinkage, without air penetration [10]. The structure and mechanical strength (i.e. the elastic modulus) of this concentrated bulk are not significantly different from those of an emulsion directly prepared at this higher concentration. Despite this phenomenon, the drying rate continuously and rapidly decreases as the water content decreases, in contrast with the drying of a simple granular packing. These results from a concentration gradient which develops towards the free surface of the sample where the oil droplets finally coalesce, ultimately forming an oil layer covering the sample through which the water molecules have to diffuse before evaporating. Moreover, as during the process, the liquid is transported towards the free surface where it evaporates, surfactants accumulate and tend to form a thin solid layer below the oil layer, which tends to further reduce the drying rate.

Here we focus on bitumen emulsion drying. We follow in particular the distribution of water and bitumen in a drying sample with the help of MRI. These data are completed with information on the rheological behavior of the emulsion at different concentrations, drying rate, and the structure evolution with time (coalescence and droplet sizes). This provides an advanced picture of the drying properties of a layer of bitumen emulsion exposed to air along one of its face.

2. Materials and methods

2.1 Material preparation

We prepared a bitumen-in-water emulsion (referred to as bitumen emulsion) using bitumen with a penetration grade 160/220, which indicates that the bitumen is “soft” or malleable at ambient temperature according to empirical characterization tests [4]. The same bitumen was fluxed with a commercial oil Oleoflux® (rapeseed derivative from EIFFAGE Infrastructures) at 15 wt% in order to highly decrease its viscosity. To do so, the bitumen is heated 2 hours at a 110°C before adding the necessary amount of fluxing agent. In the following, the non-fluxed emulsion will be also sometimes more simply described as the emulsion. The bitumen droplets are stabilized by a quaternary ammonium salt tetradecyltrimethylammonium bromide noted TTAB. The surfactant used is a quaternary ammonium salt with a critical micellar concentration (CMC) of 3.5 mM and a solubility in water of 10% (w/v), which are respectively equivalent to mass fractions of 0.12 wt% and 9.09 wt%.

The emulsions were prepared using a colloidal mill Rink Electro, a rotor-stator apparatus inducing an apparent shear rate of 14.10^3 s^{-1} (gradient of velocity, i.e. typically velocity difference between tools divided by their distance) in a 0.3 mm gap. The aqueous surfactant solution (1.14 wt%) is introduced in the colloidal mill at a temperature of 45°C and then the bitumen, preheated at 110°C for 2 hours, is progressively added. The emulsions obtained (fluxed or not fluxed) have an initial bitumen volume fraction of 68%. Note that in the following the simple notation % will correspond to volume fractions. For some experiments, the emulsion was diluted with aqueous phase to reach a volume fraction of 59%. This emulsion was stable to sedimentation for a couple hours after preparation (in absence of drying).

The size of the bitumen droplets was estimated with the help of confocal microscopy. In that aim, the emulsions were strongly diluted with distilled water containing fluorescein (Fluorescein sodium, Fluka

Chemica). Note that this dilution could not affect the droplet size. A drop of the resulting solution was deposited on a glass slide and observed with a confocal microscope (Carl Zeiss LSM 700) equipped with a 488 nm laser. The radius of the droplets was then measured using ImageJ and Matlab software and used to establish the oil droplet size distribution in volume percentage (see more details in [10]). Such a measure was carried out during the storage of the samples, to check the absence of evolution of droplet size, and during drying by extracting small amounts (typically 0.1 g) of the emulsion sample at different depths. This mass withdrawal was taken into account when following the water mass loss of the whole sample.

2. 2 Rheological behavior of bitumen emulsions

In order to analyze the material evolution during drying it is useful to have an idea of the mechanical behavior of these systems. In that aim we carried out rheological tests with a stress-controlled rheometer (Malvern Kinexus ultra+) equipped with a roughened cone and plate geometry (20 mm radius, α=4° angle and gap at the truncature g=0.15 mm). We imposed an increasing stress ramp (over 2 min) followed by a decreasing stress ramp (over the same duration). The stress was varied logarithmically to allow the observation of the material behavior in the different regimes. For a bitumen concentration below about 50% the material is clearly Newtonian: the apparent flow curves obtained for increasing and decreasing stress ramps well superimpose, indicating no thixotropy, along a straight line of slope 1 in logarithmic scale (see Figure 1a and b). For a larger concentration, say 59%, the material starts to exhibit some slight shear-thinning behavior at low shear rate, an effect more marked for the fluxed bitumen emulsion (see Figure 1b). As the concentration is further increased the behavior changes more significantly for the bitumen emulsion. Now the fluid exhibits a yield stress, below which no steady state flow may be observed. In fact the initial curve part of the increasing stress ramp (see Figure 1a) reflects the behavior of the material in its solid regime before yielding, the rheometer recording an apparent shear rate associated only to the additional deformation in this regime at a rate equal to the stress increasing rate [32]. Then we have a stress plateau, associated with the beginning of the liquid regime and finally the shear rate increases progressively with the shear stress (see Figure 1a). The decreasing curve superimposes to the increasing one along the latter region, but then decreases to a lower stress plateau. This means that the initial, apparent ("static") yield stress, is associated with the existence of some structure in the material, which breaks during flow and does not recover sufficiently rapidly during the decreasing ramp. This effect is likely due to the existence of a network of links between the droplets throughout the sample, which would break during flow and would not reform except after some time at rest. There nevertheless still exists some ("dynamic") yield stress after this breakage, which is lower than the static yield stress. This should be due to the jamming of droplets, as for simpler emulsions [33]. The fluxed bitumen emulsion seems to be simpler, exhibiting a simple yield stress fluid behavior (see Figure 1b).

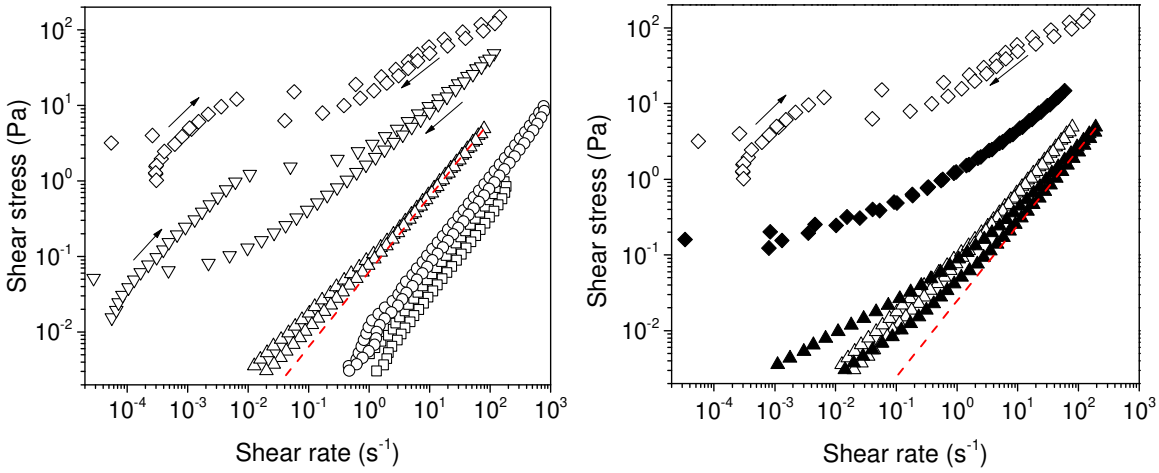

Figure 1 : Flow curves of bitumen emulsions (a and b) and fluxed bitumen emulsions (b) at different bitumen volume fractions: 39% (squares), 49% (circles), 59% (triangles), 64% (inverted triangles) and 68% (diamonds). Bitumen emulsions are represented with open symbols, fluxed bitumen emulsions with filled symbols. For each flow curve increasing and decreasing stress ramps are represented; if the ramps do not overlap, the arrows indicate the increasing and decreasing stress ramps are. The red dotted lines of slope of 1 are guide for the eye.

2.3 Drying experiments

Drying tests were performed on emulsion samples contained in glass Petri dishes (9 cm diameter, initial sample thickness: 1.5 cm). In order to limit the adherence of the material on the walls and bottom of the Petri dish, the dishes were coated beforehand with a thin layer of perfluorinated grease (Krytox GPL 205, DuPont). Negligible deposits of bitumen were observed along the wall as the sample height decreased, which confirms that the sample essentially slides along the walls. Moreover, the material appears to remain in contact with the wall over all the drying process, which means that radial contraction is negligible. This implies that such drying process may be seen as essentially a one-dimensional process, i.e. along the vertical direction, and the sample diameter has no impact on the characteristics observed per unit section area.

Since the bitumen does not evaporate during the tests the bitumen mass (M_B) in the emulsion remains constant, while the mass of water (M_W) decreases in time (t). In the absence of air inside the emulsion, a point that will be discussed later, we may then define the water volume fraction $\phi(t)$ as:

$$\phi(t) = \frac{\Omega_W}{\Omega_B + \Omega_W} \tag{1}$$

in which $\Omega_W = M_W/\rho_W$ and $\Omega_B = M_B/\rho_B$ are respectively the current water and bitumen volumes, and ρ_W and ρ_B the water and bitumen densities. From the variation of the water mass contained in the sample we can also define the drying rate V of the emulsion as:

$$V = -\frac{1}{\rho_W S}\frac{dM_W}{dt} \tag{2}$$

with S the sample surface area.

2.4 MRI measurements

The drying experiments with *in situ* monitoring of the local bitumen and water content were performed in a vertical Magnetic Resonance Imaging (MRI) spectrometer (Bruker DBX 24/80) operating at 0.5T (20MHz proton frequency) with a measuring area 20 cm wide. A MRI compliant drying setup allowed the drying of the sample directly in the MRI magnet during measurements. It consisted of a PMMA sample holder and a long vertical column through which a dry airflow was blown towards the top surface of the emulsion at a controlled rate. All experiments were carried out at room temperature (T≈22°C) and air was blown at same temperature. Proton MRI detects hydrogen atoms, therefore in the case of a bitumen emulsion, those of the water and the bitumen. Different MRI sequences are used to distinguish the two components, based on their different NMR relaxation times [33] and follow their spatial distribution in the sample. The principles of these sequences are recalled in the following. The values of the different parameters or characteristics of these sequences are presented in Table 1.

The first sequence measures the apparent water distribution along the sample vertical axis (z): we ran a one-dimensional double spin-echo sequence (two first echoes of the Carr-Purcell-Meiboom-Gill sequence [34-35], coupled with imaging gradients) on the emulsion sample. Exponential extrapolation was used to compensate spin-spin relaxation, that is to say the unbiased proton density as a function of height noted $\rho_0(z)$ and directly proportional to the amount of water contained in the sample was extrapolated as $\rho_0(z) = \rho_1^2(z)/\rho_2(z)$ where $\rho_1(z)$ and $\rho_2(z)$ are the signal proton density for the first and second echo respectively, obtained from an inverse Fourier Transform of the respective signal in the k-space. Thus, we measured the water proton density of thin cross-section layers 470 µm thick along the sample vertical axis. Bitumen proton density is not measured with this sequence as the bitumen relaxation time is very short (100 times smaller than for water) (see [36]). We disregarded data values four times lower than the standard deviation of the measured noise. In such measurements the water mass is finally simply proportional to the NMR signal, with a constant coefficient of proportionality for a series of tests with given settings of the system. Note that our entire analysis relies on the assumption that no chemical reaction occurs between water and bitumen, i.e. the two material types remain distinct. Actually, from a characterization of our bitumen (see [11]) it appears that this material contains about 20% of polar components (resins and asphaltenes), with which some chemical exchange (hydrogen bond) may be expected at some time during the process. This suggests that the possible exchange is limited but we have no means to further quantify it. Anyway, we can suggest that if such exchanges exist the corresponding (likely small) amount of water molecules would have a significantly damped mobility and thus would just simply not contribute to the NMR signal in our DE measurements, from the beginning to the end of the test.

This implies that, for a series of profiles for a drying test, the local water mass at any time can be deduced by comparison of the corresponding signal with the signal in a region where the water mass is known (typically the water mass in the sample in its initial state). This makes it possible to deduce the local (at the height *z*) water concentration at time *t* through the equation $\phi(z,t) = \left(\rho_0(z,t)/\rho_0(z,0)\right)\phi_0$, in which ϕ_0 is the initial water volume fraction. Again, this expression is valid only in the absence of air penetration.

The second MRI sequence used is a one-dimensional Single Point Imaging (SPI) sequence [37]. This sequence consists in exciting the entire sample at once, but only one data point is retrieved per excitation. The process is repeated until all necessary data points have been retrieved. The time interval between excitation and detection is kept to a minimum: this allows us to detect components

with very short relaxation times such as bitumen ($T2 \approx 1$ms). The NMR signal from SPI sequence will therefore be the sum of both bitumen and water signal, but with different factors depending on the amount of protons in each material type. Here each point of the profiles correspond to the signal in a cross-section layer 940 µm thick (along the sample vertical axis). Consequently, the decrease in total SPI signal intensity will be less than for total DE signal intensity as bitumen does not evaporate and contributes to the signal intensity throughout drying. We may therefore consider that SPI profiles are an upper bound for total water content. We also disregarded data values three times lower than the standard deviation of the measured noise.

A third MRI sequence was used to perform T1 relaxation time distribution measurements i.e. the time evolution of longitudinal magnetization when it relaxes to thermal equilibrium after an electromagnetic impulsion. To do so, the Inversion-Recovery sequence [38] is typically used, with 30 inversion times logarithmically distributed in the range 1-8000ms and a recovery time of 10s. The T1 relaxation times distribution is then obtained through an Inverse Laplace Transform [39]. This distribution typically consists of several peaks distributed at different T1 values. Roughly speaking, the T1 value is characteristic of a proton and its environment: in the case of bitumen emulsions, two peaks are expected, one for water and one for bitumen. However, in T1 relaxation time measurements, no peak is found for the bitumen as its relaxation time is too short at ambient temperature to be detected [40]. An example of such a series of measurements is shown in Appendix 1. In addition, the area beneath the peak can be considered as proportional to the amount of water as verified by comparing T1 measurements with weighing of samples of known compositions. By repeating this measurement throughout drying, the water volume fraction may be followed.

Sequence	Repetition time T_R (ms)	T_E	Number of scans	Field of view (cm)	Pixels
DE (Double Spin-Echo)	8000	4 ms (Echo time)	128	6	128
SPI (Single Point Imaging)	100	315 µs (Impulsion / Excitation)	16	6	64

Sequence	Range (ms)	Repetition time T_R (ms)	Number of points	Scans
T1 (Relaxation distribution)	1-8000	10000	30	4

Table 1: Parameters of the different sequences used in this work (see text for details on the principles of these sequences).

The three MRI sequences were repeated in cycles lasting approximately 40 min. By integration of the signal over each profile we could compute the water mass M_W in the sample as a function of time and found that all three sequences gave very similar results, confirming the robustness of the measurements (see Figure 2). As an additional control of the MRI measurements, the sample was weighted when the experiment was interrupted. The water mass measured with MRI and that deduced from weighing are in good agreement (see Figure 2), confirming that all water contained in the sample is effectively detected by MRI at the different concentrations tested during the process.

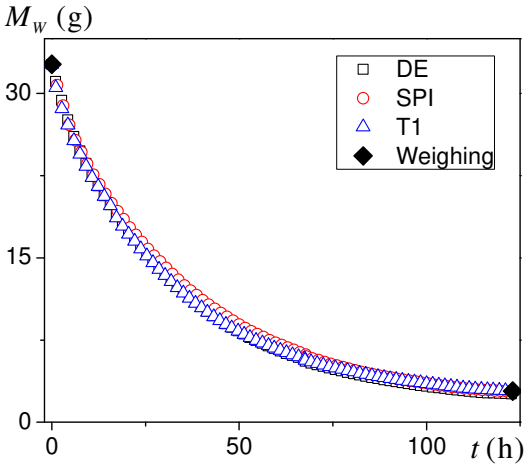

Figure 2 : Evolution of the total mass of water of a 59% bitumen emulsion during drying obtained through weighing and MRI measurements (through different techniques, see text).

In addition, two dimensional (2D) images were obtained with the MRI apparatus using 2D NMR slice-selective spin-echo imaging; these images are therefore T1-weighted. An echo time T_E of 6.54 ms was used, with a repetition time T_R of 1000ms. The field of view chosen was 13.0 (width) x 6.5 (height) cm², and the matrix size 128 x 128 pixels x pixels. In the images presented here the brighter regions correspond to larger water density. Note that due to the technique used this only provides a qualitative view of the water density distribution in the sample. Quantitative data are obtained from the above described sequences.

3. Results and discussion

3.1 Qualitative observations

Initially the emulsion sample fills the Petri dish in which it has been placed. During drying, no radial contraction of the emulsion is observed, i.e. the emulsion remains in contact with the side walls, while its thickness decreases approximately uniformly. This means that on average, water (either in vapor or liquid form) is transported along the sample axis up to the free surface, i.e. we are dealing with a unidirectional drying process. We thus expect that at any time the characteristics of the process are similar at different points situated at the same distance (height) from the bottom, so that a measure of some mean property in a thin cross-sectional layer at a given height reflects the local value of this property.

The emulsion is initially light brown (see Figure 3a and a'). Quickly after the beginning of drying, we observe, say from a concentration around 62%, the formation of a dark elastic layer at the free surface as already observed in [9] (see Figure 3b'). This layer seems to thicken slightly during drying (up to about 2 mm) while, progressively, the rest of the material darkens (see Figure 3b) and becomes pasty: typically, beyond 64% the material is unable to flow unless you apply some force on it. As the emulsion goes on drying it becomes harder to distinguish two layers, and ultimately, when the sample mass no longer evolves we obtain what appears to be a homogeneous sample.

Regular sampling of the two layers and observation with the confocal microscope show that they are composed of distinct bitumen droplets that are progressively pushed together as the emulsion shrinks: the droplets easily disperse in water and their grain size distribution remains constant (see Appendix 2). This result is especially remarkable for the surface layer, which is just a highly concentrated bitumen emulsion layer. The progressive increase of the bitumen droplet concentration is consistent with the observation that the size of the pores occupied by water progressively decreases, as may be seen from the relaxation time distribution: the relaxation time of the main peak of the distribution decreases in time, corresponding to a decreasing pore size (see Appendix 1).

The bitumen droplets remain distinct until the water content drops to about 15% (on average, which means that the surface layer concentration is likely lower): for this concentration a sample taken from the surface layer can no longer be dispersed in water by a simple hand mixing, indicating that the bitumen droplets have coalesced. At the same time, a sample taken from the bulk can only be partially dispersed in water. Let us insist on the fact that this 15% limit is a rough approximation as we only followed the structure evolution at some concentrations separated by several percents, and this value only reflects the average concentration reached at some time without taking into account the concentration gradient. Therefore, we can conclude that during a long period of drying, the emulsion essentially concentrates with some concentration gradient, and below some critical concentration, the droplets begin to coalesce.

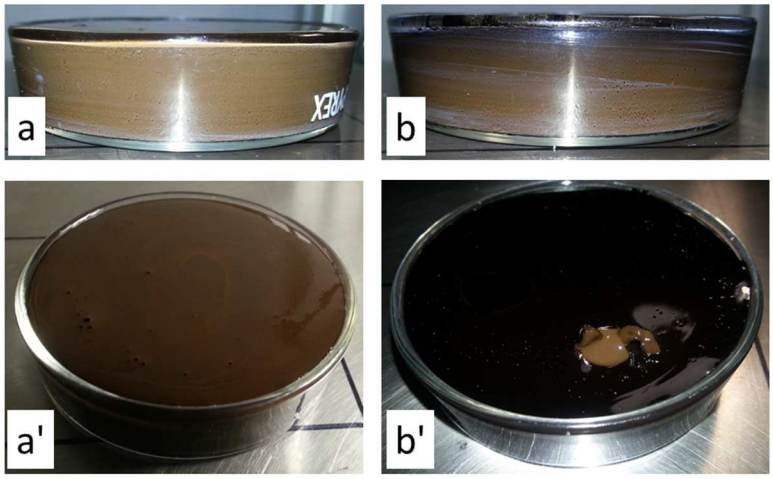

Figure 3 : Aspect of drying a bitumen emulsion initially composed of 59% bitumen at different stages. View from the side (top row) and from above (bottom row): (a) and (a') Initial state (*t*=0) $\phi = 59\%$; (b) (*t*=31h30) $\phi = 36\%$. The Petri dish has here a height of 1.5 cm and a diameter of 5.5 cm. In (b') a piece of the top layer has been removed to show the color of the sample below.

3.2 Local observations

From MRI we obtain images along a longitudinal cross-section, which gives a qualitative idea of how the drying develops in the 59% emulsion. We see that during a first period for which the water content is decreased by a factor about two, a low concentration front progresses in the sample, while the rest of the material remains approximately in its initial state (i.e. at its initial concentration) (see the three first pictures of Figure 4). In the next step, i.e. when this front has reached the sample bottom, the

water concentration appears to decrease homogeneously in the whole sample (see the last three pictures of Figure 4). Note that throughout the process the sample shrinks vertically. The dynamics of the low concentration (dark) front and the sample thickness as they appear from these pictures are consistent with the profiles of Figure 7: at a concentration of 33% the apparent sample thickness is 1.15 cm and the dark region thickness 0.35 cm; at a concentration of 29% the apparent sample thickness is 1.05 cm and the dark region thickness 0.63 cm; at a concentration of 22% the apparent sample thickness is 1.00 cm. These values are close to respectively the apparent width of the profile and the width of the step progressing from the left of the profile.

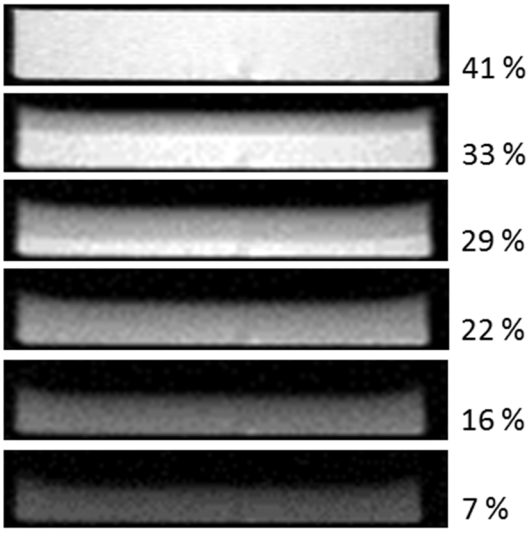

Figure 4: 2D MRI images of the drying of a bitumen emulsion sample (initial concentration: 59% bitumen) at different stages: the mean water fraction is indicated on the right.

Through DE profiles measurements we obtain the successive distribution profiles of water in time for our sample. Let us focus on the typical example of the drying of the 59% fluxed bitumen emulsion. The DE profiles, which correspond strictly to the water distribution in the sample, initially exhibit a step that propagates downwards. Some water near the surface evaporates, inducing a lower water fraction in a region close to the free surface, while the water fraction remains almost uniform in the rest of the sample (see Figure 5a). This water-depleted area progresses through the emulsion sample in the form of a step until it reaches the bottom after 25 hours of drying, which corresponds to a total water fraction of 25%. The water content then decreases in a more homogeneous manner over the whole height of the sample, albeit with a slight gradient: the water fraction remains higher towards the bottom of sample than near the sample free surface.

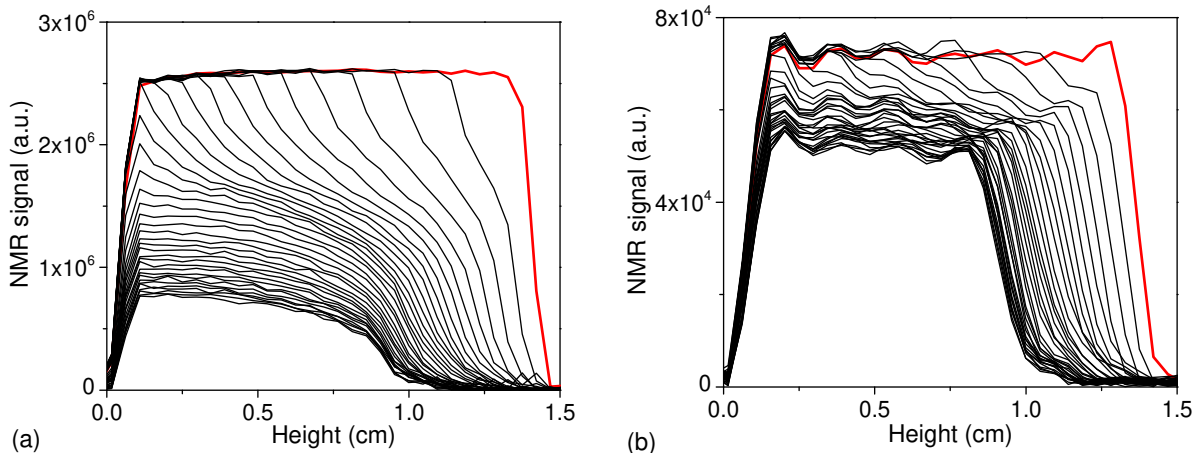

Figure 5: DE (a) and SPI (b) profiles (respective resolution: (DE) 0.47 mm, (SPI) 0.94 mm) of the drying of a fluxed bitumen emulsion initially composed of 59% bitumen and containing 1.14 wt% surfactant in aqueous phase (H=1.4 cm, air flow 0.1 $m.s^{-1}$). The NMR signal is represented as a function of height, the bottom of sample being located on the left-hand side of the graph and the sample surface exposed to air flow on the right-hand side of the graph. The initial profile is represented with a thick red line; subsequent profiles are represented every 100 min after beginning of drying.

Interestingly, for this material, when using the SPI sequence, the MRI signal from bitumen is sufficiently large compared to that of water, so that the SPI profiles give us a clear view of the distribution of both materials in space during the process. In particular, we again see some step in the profile, progressing downwards, which corresponds to the step in the water (DE) profiles as described above (see Figure 5b). The profile level then decreases approximately evenly.

Throughout the process, the emulsion shrinks. A first question is then whether some air penetrates the sample or not. This problem can be addressed with the help of the set of both DE and SPI data. Indeed, from the water profiles we can deduce the amount of water that has disappeared from the sample at each time. In that aim we integrate the MRI profile and compare the resulting value to the integral of the first profile, thus deducing the fraction of water evaporated. This evaporated amount can be translated in a thickness reduction, assuming negligible air penetration, and we deduce the effective sample thickness under these conditions. Moreover, we can measure the apparent thickness of the sample from the SPI profiles, from the width of the DE (water) profile taken for example at half the profile height. The general uncertainty on these measures is about 15%. The thickness estimated by assuming no air penetration appears to be close to the effective thickness (see Figure 6), which confirms that negligible air penetrates the sample during drying.

Another important question is whether some fully dry (i.e. without water) region develops close to the free surface. In order to test that point we can compare the thickness of the water profile (from DE measurements) and that of the sample (from SPI measurements). Some slight difference can be observed (see Figure 6), but there is no clear trend, such as a progressive increase of a dry region. This suggests that the differences only result from the uncertainty on data and more particularly on the exact profile shape close the free surface. Thus, we conclude that if some dry region forms close to the

free surface its thickness is very small, typically less than a few hundred microns, which corresponds approximately to our MRI resolution

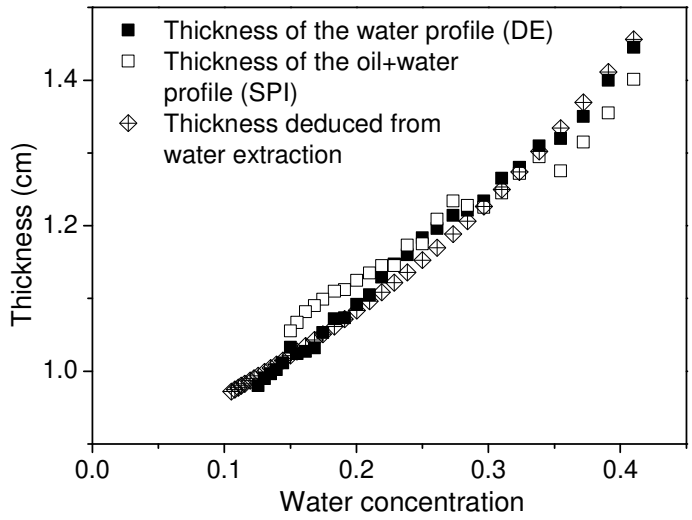

Figure 6: Evolution of the thickness of DE profiles, SPI profiles and deduced from water extraction as a function of the global water concentration in the sample for the drying of a fluxed bitumen emulsion initially composed of 59% bitumen and containing 1.14 wt% surfactant in aqueous phase (H=1.4 cm, air flow 0.1 $m.s^{-1}$).

Similar results are obtained for the non-fluxed bitumen emulsion (see Figure 7) although the determination of the sample thickness from SPI measurements is more uncertain because in that case the NMR signal from bitumen droplets is much lower than that from water, so that the SPI profiles appear rather similar to the DE profiles (see Appendix 3). Nevertheless, the sets of water profiles in time are quite similar for the fluxed and non-fluxed bitumen emulsions (see Figure 5 and Figure 7),

suggesting similar global processes (with in particular no air penetration and negligible dry region at the free surface).

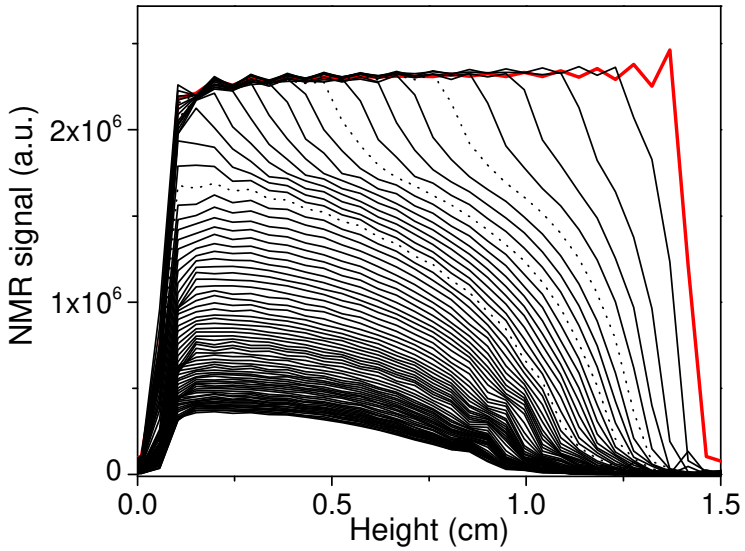

Figure 7: DE profiles of the drying of a bitumen emulsion initially composed of 59% bitumen and containing 1.14 wt% surfactant in aqueous phase (H=1.4 cm, air flow 0.1 $m.s^{-1}$). The initial profile is represented with a thick red line; subsequent profiles are represented every 97 min after beginning of drying. The dotted lines correspond (from right to left) to the water concentrations (respectively 33%, 29% and 22%) at which the images of Figure 4 were obtained.

For a higher initial bitumen concentration there is only a slight effect of step propagation at the beginning, which in fact could also be considered as the development of the water concentration gradient up to the bottom (see Figure 8). Afterwards, the profiles evolve in a way similar to that for a lower initial bitumen concentration. This similarity may be further illustrated through a comparison of the profiles measured at different times for the two different initial bitumen emulsions but associated with the same current water fraction. It appears that despite significant concentration gradients the profiles are very close to each other (see Figure 9).

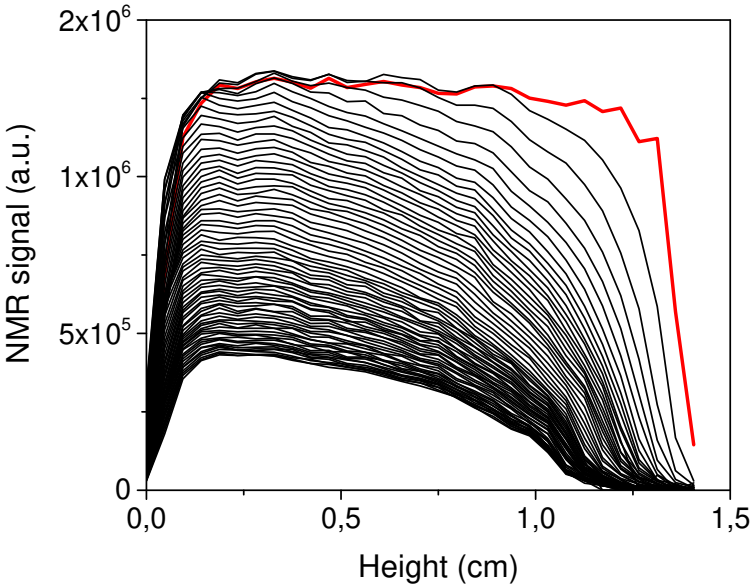

Figure 8: DE profiles of the drying of a bitumen emulsion initially composed of 68% bitumen and containing 1.14 wt% surfactant in aqueous phase (H=1.3 cm, air flow 0.1 m.s^{-1}). The initial profile is represented with a thick red line; subsequent profiles are represented every 1 h after beginning of drying.

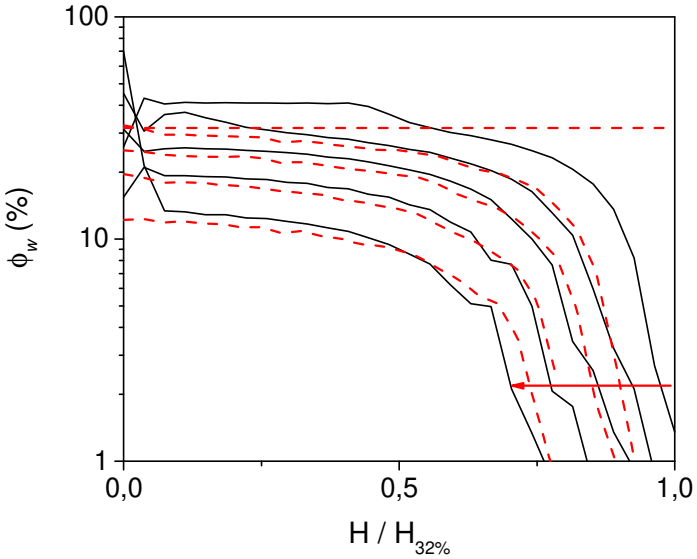

Figure 9: Water concentration profiles of drying bitumen emulsions with different initial compositions (b) 59% (black full lines) and 68% (red dotted lines) bitumen emulsions containing 1.14 wt% in aqueous phase. Profiles for different water contents are represented (from top to bottom, 32-25-20-15-10%) as a function of height normalized by $H_{32\%}$, the profile height at $\phi = 32\%$.The red arrows indicate the evolution in time.

3.3 Drying rate

The drying rate for our different tests may be computed from MRI data. More specifically, we integrate the water profiles and by comparison with the initial one, deduce the water mass loss since the test beginning. The current water concentration and drying rate can then be computed through equations (1) and (2).

First, we see that the drying rate does not exhibit any constant rate period, it immediately and continuously decreases in time (see Figure 10). This may also be observed from the mass vs time evolution deduced from different NMR measurements types (see Figure 2).

The second remarkable feature is that around a water concentration of 22% the drying rate curves associated with different initial concentrations of bitumen or different types of bitumen, gather and then superimpose for any lower concentration. In other words, the drying rate is thus now independent of the initial emulsion concentration. Also note that there is no significant difference between the drying rate curves obtained for the two types of bitumen emulsion (fluxed or not).

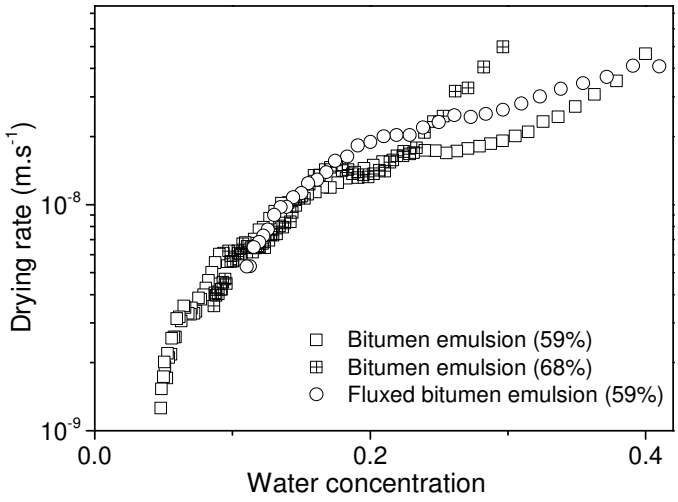

Figure 10: Drying rate as a function of water volume fraction for different types of bitumen emulsions at different initial bitumen concentrations (indicated in brackets).

4. Further analysis

Overall, our observations show that the drying of a bitumen emulsion leads to the shrinkage of the sample, with a heterogeneous decrease in water content throughout the emulsion. If the initial bitumen concentration is not sufficiently high, first a rearrangement of the droplets (the step propagation effect), leading them to reach a jammed configuration. This effect appears to be consistent with the rheological trends of these materials: for an initial bitumen concentration of 59% the material does not exhibit a yield stress (see Figure 1), which means that the droplets are not jammed in a network occupying the whole sample. However, such a network appears when increasing the concentration as shown from rheometrical tests at higher concentrations: a yield stress now appears which increases with the bitumen fraction (see Figure 1). We can thus consider that at 59% initial bitumen fraction it is still relatively easy to rearrange the droplets to extract some water and

then reach a slightly larger concentration, which explains the formation of the step front: water is directly extracted from the top of the sample up to a critical concentration at which the droplets start to be jammed. The step then progresses further downwards in the sample gathering the droplets up to the jammed configuration at larger depth.

When the step front has reached the sample bottom, any further extraction of water implies some gathering of the droplets beyond the critical jamming concentration. Now a simple rearrangement of the droplet configuration is not sufficient, one needs to somewhat deform the droplets. This effect will then develop with some gradient, as expected from a poroelastic problem [41]: the water extraction induces some internal pressure on the droplets close to the free surface, which propagates more or less rapidly and easily downwards. In this context it is remarkable that the water profiles reached by the emulsion during drying solely depend on the current water fraction.

Let us now examine the dynamics of the process. Since here no dry region tends to develops around the free surface as for standard solid porous materials during the second stage of drying, we deduce that the decrease of the drying rate, occurring immediately when drying begins, is neither due to some evaporation of water at an increasing distance from the sample free surface, nor to the diffusion of water through a pure bitumen layer of growing size (an effect which was observed for simple oil in water emulsions [10]). Due to the water content gradient developing in the sample we deduce that the decrease of the drying rate is basically due to the reduction of the number and size of water paths towards the sample free surface where evaporation occurs. We know that the constant drying rate period for simple porous medium results from the sufficient amount of liquid patches remaining along the free surface [42-43]: the evaporation is thus constant and a sufficient liquid network through the sample constantly feeds the liquid patches. Here we can assume that simultaneously, the emulsion surface covered by the patches decreases and the liquid network becomes more tenuous during drying. It seems difficult to further elaborate the analysis beyond these basic qualitative concepts. This is quite different from the drying of silicone oil emulsions, for which we observed the formation of a concentrated oil layer composed of coalesced oil droplets, through which water has to diffuse and which effectively slows drying down as it becomes thicker [10].

Thus, we have a continuously decreasing drying rate, whose variations can hardly be predicted quantitatively. After the initial stage during which the droplets essentially gather to a jammed configuration, the drying rate follows a master curve, whatever the initial bitumen concentration. We observed that, at the same time, we have a unique water content distribution. This further supports the idea that the water network through the sample imposes the drying rate: the similar liquid network thus gives a similar drying rate for the different emulsions studied.

5. Conclusion

From Magnetic Resonance Imaging (MRI) we were able to show that bitumen emulsions essentially dry homogeneously, with nevertheless a slight concentration gradient increasing towards the sample free surface exposed to air. Except in the very last stages of drying the bitumen droplets do not coalesce. In parallel the drying rate strongly and continuously decreases, which is attributed to the reduction of the hydraulic network connected to the sample free surface. It appears that the evolution of the drying rate is independent of the initial droplet concentration, i.e. it varies in the same way as a function of the current water content, and the water concentration distribution is also apparently

essentially a simple function of the current water content. Note that these conclusions are valid in our range of experimental conditions, in particular for an air flux in a limited range.

These results cannot directly be used for the applications on roads, and further studies of the drying of bitumen emulsion in a granular packing have to be carried out. Nevertheless the present results already suggest that the drying of bitumen emulsions inside granular packing will be much more complex that simple liquids which are moved towards the free surface of the sample by capillary effects. It is likely that, while drying takes place, which leads to an increase of the concentration of the bitumen emulsion, this emulsion will soon become more viscous and thus unable to be transported towards the free surface. Moreover the present observations show that the evaporation rate of the emulsion, inside or even along the sample free surface, will be lowered by the formation of the highly concentrated bitumen layer along the air-emulsion interface.

It remains that the drying of bitumen emulsions is a complex field, due to the various physical effects that might occur at the different stages of the process and leading to strong material heterogeneities. Further studies in relation to the application for road pavements should also attempt to determine how the basic trends described here may be affected by some preliminary destabilization of the bitumen emulsion by a chemical agent or by the presence of reactive aggregates in the road pavement mix.

Appendix 1: T1 relaxation time distribution during drying of a 59% bitumen emulsion

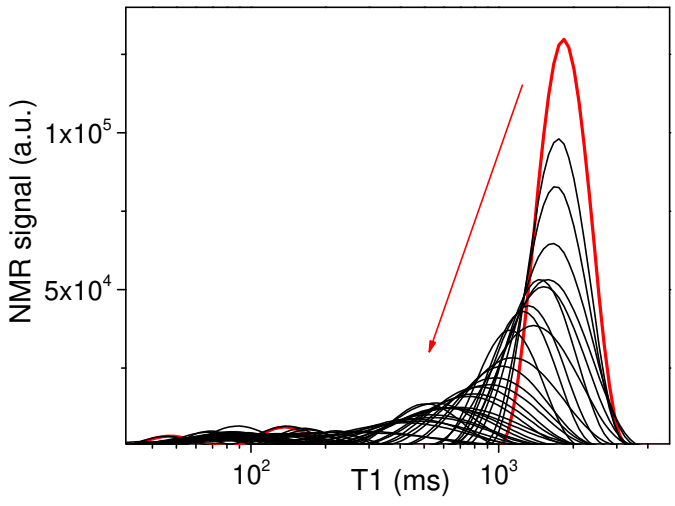

Figure A1: T1 relaxation time distribution profiles of the drying of a bitumen emulsion initially composed of 59% bitumen and containing 1.14%$_{wt}$ surfactant in aqueous phase (H=1.4 cm, air flow 0.1 m.s^{-1}). The initial distribution is represented with a thick red line; subsequent profiles are represented every 1 h after beginning of drying, following the red arrow.

Appendix 2: Bitumen droplet size evolution

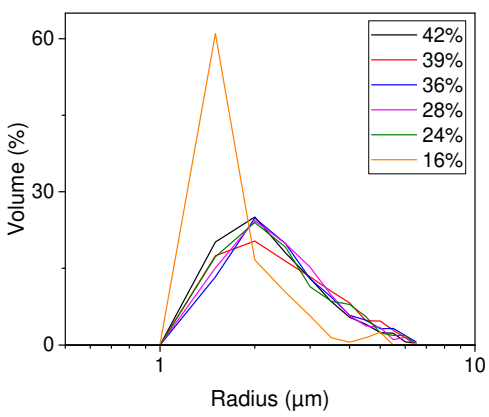

(a)

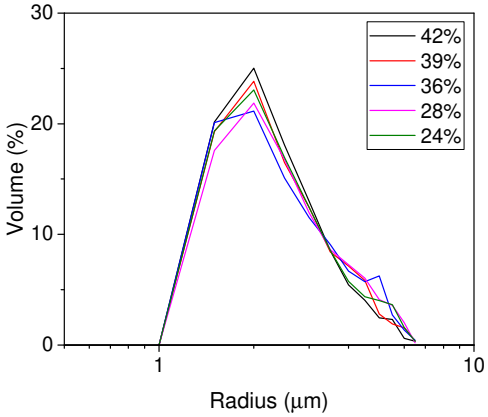

(b)

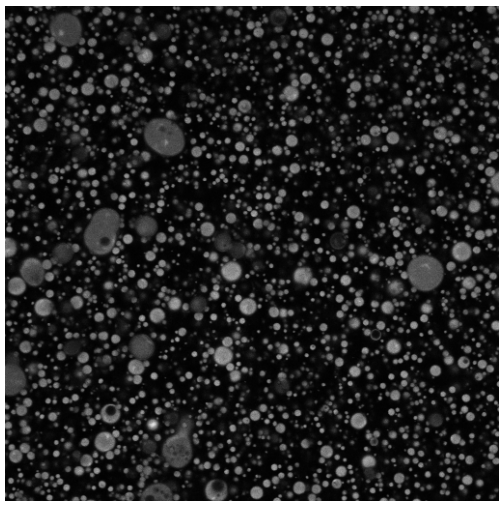

(c)

Figure A2: Evolution of droplet size distribution of the bulk (a) and surface layer (b) of a drying 59% bitumen emulsion. The water volume fractions of the emulsion when it was sampled are indicated in the legend of both samples. Note that for 16% the droplets in fact seem to have started to coalesce. (c) Aspect of the emulsion structure for a bitumen emulsion during drying when the water volume fraction was 25%.

Appendix 3: SPI profiles of drying 59% bitumen emulsion

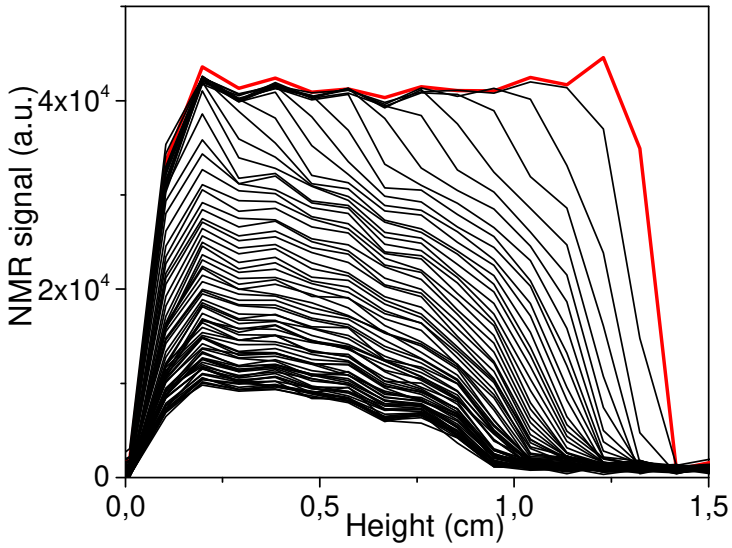

Figure A3: SPI profiles of the drying of a bitumen emulsion initially composed of 59% bitumen and containing 1.14%$_{wt}$ surfactant in aqueous phase (H=1.4 cm, air flow 0.1 m.s^{-1}). The initial profile is represented with a thick red line; subsequent profiles are represented every 97 min after beginning of drying.

6. References

[1] A. Motamed, D. Salomon, N. Sakib, A. Bhasin, Emulsified Asphalt Residue Recovery and Characterization Combined Use of Moisture Analyzer Balance and Dynamic Shear Rheometer, Transportation Research Record, 2444 (2014) 88-96

[2] M. Guirguis and A. Buss, Performance Evaluation of Emulsion and Hot Asphalt Cement Chip Seal Pavements, J. Mater. Civ. Eng., 29 (2017) 04017202

[3] M.-C. Liao, C.-C. Luo, T.-Y. Wang, and X. Xie, Developing Effective Test Methods for Evaluating Cold-Mix Asphalt Patching Materials, J. Mater. Civ. Eng., 28 (2016) 04016108

[4] J.-F. Corté and H. Di Benedetto, Road asphalt materials – components and thermomechanical properties, Hermes Sciences Publications, Paris, 2004 (in French)

[5] G.J. Prakash, P. Mahabir, and S.U. Chandra, Performance of Bituminous Mixes Containing Emulsion-Treated Recycled Concrete Aggregates, J. Mater. Civ. Eng., 30 (2018) 04018052

[6] Y. Wang, Z. Leng, X. Li, and C. Hu, Cold recycling of reclaimed asphalt pavement towards improved engineering performance, J. Clean. Prod., 171 (2018) 1031–1038

[7] S. Panda, K. Pal, S. Merzara, M.R. Gray, Q. Liu, P. Choi, Transport and removal of a solvent in porous media in the presence of bitumen, a highly viscous solute, Chem. Eng. Sci., 165 (2017) 229-239

[8] V. S. Ryabenko, E. A. Chigorina, A. L. Razinov, Y. A. Ubaskina, and I. D. Kovtun, The Preparation of the Quick-Drying Bitumen Emulsion for the Protection of the Road Surface Asphalt Concrete Layer, Orient. J. Chem., 32 (2016) 3129–3134

[9] D. Lesueur, C. Coupé, M. Ezzarougui, M. Skin Formation during the Drying of a Bitumen Emulsion, Road Mater. Pavement Des., 2 (2001) 161–179.

[10] M. Goavec, S. Rodts, V. Gaudefroy, M. Coquil, E. Keita, J. Goyon, X. Chateau, P. Coussot, Strengthening and drying rate of a drying emulsion layer, Soft Matter, 14 (2018) 8612–8626

[11] L. Boucard, V. Gaudefroy, E. Chailleux, F. Farcas, V. Schmitt, Bitumen Emulsion Destabilization Kinetics: Importance of the Crystallized Wax Content, Langmuir, 33 (2017) 9740–9749, DOI:10.1021/acs.langmuir.7b01578

[12] J. Van Brakel, Mass transfer in convective drying, in *Advances in Drying* (Mujumdar A.S. (editor), Hemisphere Pub. Corp.), 1 (1980) 217-267

[13] J.B. Laurindo, M. Prat, Numerical and experimental network study of evaporation in capillary porous media. Drying rates, *Chem. Eng. Sci.,* 53 (1998) 2257-2269

[14] I. N. Tsimpanogiannis, Y. C. Yortsos, S. Poulou, N. Kanellopoulos, A.K. Stubos, Scaling theory of drying in porous media Physical Review E, vol. 59 (1999) 4353-4365

[15] P. Coussot, Scaling approach of the convective drying of a porous medium, Eur. Phys. J. B, 15 (2000) 557–566

[16] L. Pel, H. Brocken, K. Kopinga, Determination of moisture diffusivity in porous media using moisture concentration profiles, Int. J. Heat Mass Transfer, 39 (1996) 1273-1280

[17] V. Voronina, L. Pel, K. Kopinga, Effect of osmotic pressure on salt extraction by a poultice, Construction and Building Materials, 53 (2014) 432-438

[18] D. Or, P. Lehmann, E. Shahraeeni, and N. Shokri, Advances in Soil Evaporation Physics-A Review, Vadose Zone J. 12 (2013) 11

[19] N. Shokri, D. Or, What determines drying rates at the onset of diffusion controlled stage-2 evaporation from porous media?, Water Resources Research, 47 (2011) W09513

[20] J. Thiery, S. Rodts, D. A. Weitz, and P. Coussot, Drying regimes in homogeneous porous media from macro- to nanoscale, Phys. Rev. Fluids, 2 (2017) 074201

[21] J.-P. Gorce, D. Bovey, P. J. McDonald, P. Palasz, D. Taylor, J. L. Keddie, Vertical water distribution during the drying of polymer films cast from aqueous emulsions, *Eur. Phys. J. E*, 8 (2002) 421–429

[22] D. Guigner, C. Fischer, Y. Holl, Film Formation from Concentrated Reactive Silicone Emulsions. 1. Drying Mechanism, *Langmuir*, 17 (2001) 3598‑3606

[23] D. Guigner, C. Fischer, Y. Holl, Film Formation from Concentrated Reactive Silicone Emulsions. 2. Surfactant Distribution, *Langmuir*, 17 (2001) 6419‑6425

[24] D. Guigner, C. Fischer, Y. Holl, Film formation from concentrated reactive silicone emulsion: 3. film structuring, *Polym. Int.*, 52 (2003) 448‑456

[25] H. Feng, J. Sprakel, D. Ershov, T. Krebs, M. A. C. Stuart, J. van der Gucht, Two modes of phase inversion in a drying emulsion, *Soft Matter*, 9 (2013) 2810‑2815

[26] H. Feng, J. Sprakel, J. van der Gucht, Hydrodynamic model for drying emulsions, *Phys. Rev. E*, 92 (2015) 023011

[27] K. Hasegawa, S. Inasawa, Kinetics in directional drying of water that contains deformable non-volatile oil droplets, *Soft Matter*, 39 (2017) 7026-7033

[28] E. Ciampi, U. Goerke, J. L. Keddie, P. J. McDonald, Lateral transport of water during drying of alkyd emulsions, *Langmuir*, 16 (2000) 1057‑1065

[29] J. D. Griffith, A. E. Bayly, M. L. Johns, Magnetic resonance studies of detergent drop drying, *Chem. Eng. Sci.*, 63 (2008) 3449‑3456

[30] J. D. Griffith, J. Mitchell, A. E. Bayly, M. L. Johns, In situ monitoring of the microstructure of detergent drops during drying using a rapid nuclear magnetic resonance diffusion measurement, *J. Mater. Sci.*, 44 (2009) 4587‑4592

[31] H. M. van der Kooij, M. de Kool, J. van der Gucht, J. Sprakel, Coalescence, Cracking, and Crack Healing in Drying Dispersion Droplets, *Langmuir*, 2015, 31, 4419‑4428

[32] P. Coussot, Rheometry of Pastes, Suspensions, and Granular Materials, John Wiley & Sons, New York, 2005.

[33] G. Ovarlez, S. Rodts, A. Ragouilliaux, P. Coussot, J. Goyon, and A. Colin, Wide-gap Couette flows of dense emulsions: Local concentration measurements, and comparison between macroscopic and local constitutive law measurements through magnetic resonance imaging, Phys. Rev. E, 78 (2008) 036307

[34] H.Y. Carr and E. M. Purcell, Effects of Diffusion on Free Precession in Nuclear Magnetic Resonance Experiments, Phys. Rev., 94 (1954) 630–638

[35] S. Meiboom and D. Gill, Modified Spin-Echo Method for Measuring Nuclear Relaxation Times, Rev. Sci. Instrum., 29 (1958) 688–691

[36] M. Goavec, Drying of road materials containing bitumen emulsions, PhD thesis, Univ. Paris-Est, 2018 (in French)

[37] S. Emid and J. H. N. Creyghton, High resolution NMR imaging in solids, Physica BC, 128 (1985) 81–83 doi.org/10.1016/0378-4363(85)90087-7

[38] P. T. Callaghan, *Principles of Nuclear Magnetic Resonance Microscopy*. Clarendon Press, New York, 1993

[39] P. F. Faure and S. Rodts, Proton NMR relaxation as a probe for setting cement pastes, Magn. Reson. Imaging, 26 (2008) 1183–1196

[40] J. Dolinsek, P. Jeglic, T. Apih, G. Lahajnar, O. Naglic, and A. Sever, Temperature-dependent bitumen softening studied by NMR, J. Phys. Appl. Phys., 33 (2000) 1615 doi.org/10.1088/0022-3727/33/13/310

[41] O. Coussy, *Mechanics and Physics of Porous Solids*. John Wiley & Sons, New York, 2011

[42] E. Shahraeeni, P. Lehmann, D. Or, Coupling of evaporative fluxes from drying porous surfaceswith air boundary layer: Characteristics of evaporation from discrete pores, Water Resources Research, 48 (2012) W09525

[43] P. Lehmann, D. Or, Effect of wetness patchiness on evaporation dynamics from drying porous surfaces, Water Resources Research, 49 (2013) 8250

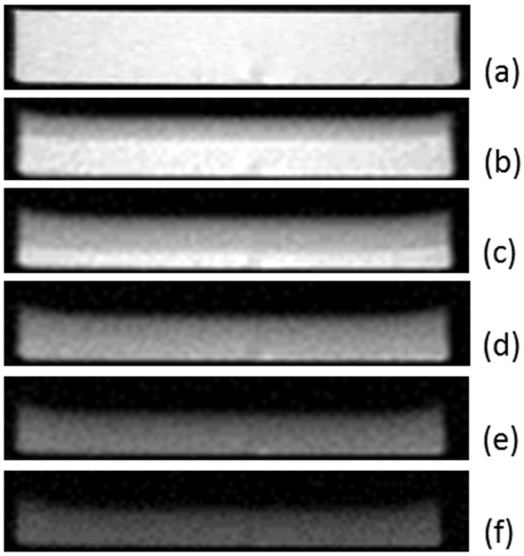

2D MRI images of the drying of a bitumen emulsion sample (initial concentration: 59% bitumen) at different stages: (water fraction) (a) 41%, (b) 33%, (c) 29%, (d) 22%, (e) 16%, (f) 7%.